STRUCTURAL BIOLOGY

Structural basis for coupling protein transport and N-glycosylation at the mammalian endoplasmic reticulum

Katharina Braunger,[1]* Stefan Pfeffer,[2]*† Shiteshu Shrimal,[3] Reid Gilmore,[3] Otto Berninghausen,[1] Elisabet C. Mandon,[3] Thomas Becker,[1] Friedrich Förster,[4]† Roland Beckmann[1]†

Protein synthesis, transport, and N-glycosylation are coupled at the mammalian endoplasmic reticulum by complex formation of a ribosome, the Sec61 protein-conducting channel, and oligosaccharyltransferase (OST). Here we used different cryo–electron microscopy approaches to determine structures of native and solubilized ribosome-Sec61-OST complexes. A molecular model for the catalytic OST subunit STT3A (staurosporine and temperature sensitive 3A) revealed how it is integrated into the OST and how STT3-paralog specificity for translocon-associated OST is achieved. The OST subunit DC2 was placed at the interface between Sec61 and STT3A, where it acts as a versatile module for recruitment of STT3A-containing OST to the ribosome-Sec61 complex. This detailed structural view on the molecular architecture of the cotranslational machinery for N-glycosylation provides the basis for a mechanistic understanding of glycoprotein biogenesis at the endoplasmic reticulum.

The mammalian translocon is responsible for cotranslational insertion of proteins into the endoplasmic reticulum (ER). The translocon is formed from the Sec61 complex, the oligosaccharyltransferase (OST) complex, and the translocon-associated protein (TRAP) complex (1). The Sec61 channel enables signal sequence–dependent protein translocation of soluble proteins through its central pore as well as integration of transmembrane proteins into the lipid bilayer through a lateral gate (2–5). OST catalyzes N-linked glycosylation of asparagine residues, an essential covalent protein modification (6–8). In higher eukaryotes, the catalytic OST subunit STT3 (staurosporine and temperature sensitive 3) is present in two paralogous forms (STT3A and STT3B) that assemble with a partially overlapping set of accessory subunits (Fig. 1A): RPN1 (ribophorin 1), RPN2 (ribophorin 2), OST48 (OST 48-kDa subunit), DAD1 (defender against cell death 1), TMEM258 (transmembrane protein 258), and OST4 (OST 4-kDa subunit) (9). STT3B complexes contain several specific subunits that include the paralogous oxidoreductases TUSC3 (tumor suppressor candidate 3) and MAGT1 (mag-

nesium transporter protein 1), whereas DC2 and KCP2 (keratinocyte-associated protein 2) are found only in STT3A complexes (10). The STT3A complex is thought to act cotranslationally and to be stably integrated into the translocon (10). The STT3B complex acts as a proofreader for sites missed by STT3A (11). Structures of monomeric bacterial and archaeal STT3 homologs have provided detailed insights into the catalytic mechanism (12–14). Genetic and biochemical data, as well as very recent high-resolution yeast OST structures (15, 16), indicate three subcomplexes of intimately interacting OST subunits. In the mammalian STT3A complex, these are RPN1 and TMEM258 (subcomplex I); STT3A, OST4, DC2, and KCP2 (subcomplex II); and RPN2, DAD1, and OST48 (subcomplex III) (7). The overall structure of mammalian OST in a native membrane environment has been established by cryo–electron tomography (cryo-ET) at medium resolution (1, 17–19); however, neither revealed structural details or the basis of STT3-paralog specificity.

To confirm STT3-paralog specificity in the ribosome translocon complex (RTC), we analyzed microsomes isolated from established ΔSTT3A and ΔSTT3B HEK cell lines, which do not express STT3A and STTB, respectively (10), using cryo-ET. Immunoblots confirmed the absence of either STT3A or STT3B in the microsomal preparations of knockout cell lines, whereas both paralogs were present in microsomes prepared from control cells (Fig. 1B). Cryo-ET and in silico analysis of subtomograms showed that control microsomes harbored translocon populations that either included only TRAP (58%) or included both TRAP and OST (42%; Fig. 1C), as expected (17–19). The same

populations were found in a similar ratio in microsomes isolated from ΔSTT3B cells (Fig. 1D), suggesting that translocon-associated OST was not affected by STT3B knockout. By contrast, no translocon-associated OST was observed after STT3A knockout (Fig. 1E), further indicating that RTCs harbor exclusively STT3A complexes (11). Instead of the TRAP-OST translocon complexes, a different, possibly partially assembled translocon population was observed after STT3A knockout.

We used single-particle cryo–electron microscopy (cryo-EM) to visualize solubilized mammalian RTCs translating the well-studied membrane glycoprotein bovine opsin (20) (figs. S1 and S2). Reconstructions yielded nonprogrammed and programmed RTCs showing an overall translocon architecture as observed in the native membrane (18, 19) except for TRAP, which appeared disordered or bound in substoichiometric amounts. Local resolution ranged from 3.5 to 4.5 Å for Sec61 and adjacent OST transmembrane helices (TMs) to 5 to 5.5 Å for more peripheral OST TMs (fig. S3). In the programmed, peptidyl-tRNA–containing complex, the nascent polypeptide density could be traced from the peptidyl (P)–site tRNA through the vestibule of the ribosomal tunnel projecting toward the cytoplasmic tip of Sec61α TM10 (fig. S4). Sec61 was in a conformation very similar to the previously described "primed" state (Fig. 2, A and B, and fig. S5) (21), with a closed lateral gate (22, 23) and the plug helix (24) occluding the central pore.

Importantly, 28 additional TMs packed against Sec61 (Fig. 2, A and B), where OST is positioned in the native translocon (19). We generated a molecular model for mammalian STT3A, revealing high structural similarity to its fungal, archaeal, and bacterial homologs (fig. S6) as well as its orientation in context of the RTC (Fig. 2, C and D, and fig. S6). Clear density for the pyrophosphate group of the dolichol carrier was visible in the catalytic site (Fig. 2, B to D, and fig. S3D), suggesting that STT3A was in an active state. Glycosylation of the two consensus motifs in our substrate had already been completed (fig. S1C), and no peptide-substrate density was visible in the catalytic site. The TMs assigned to STT3A were surrounded by 15 additional TMs (Fig. 2, B and C, and fig. S7A). Of these TMs, 10 were located at the distal side of STT3A, facing away from Sec61. Three of them formed a bundle directly adjacent to STT3A TMs 1 and 2, whereas another bundle of seven TMs was in proximity to STT3A TMs 5 to 8. On the basis of the three established OST subcomplexes (7) and the number of TMs included in the bundles, we assigned the three-TM bundle to subcomplex I and the seven-TM bundle to subcomplex III. One TM of subcomplex I extended into the metazoan-specific cytoplasmic domain of RPN1, which formed a four-helix bundle according to secondary-structure predictions (fig. S7, B and C). It was intercalated between the OST TMs and the ribosome and contacted the linker between ribosomal RNA (rRNA) helix H19 and H20, rRNA expansion segment ES7a (H25), and the tail of ribosomal

[1]Department of Biochemistry, Gene Center and Center for Integrated Protein Science Munich, University of Munich, 81377 Munich, Germany. [2]Department of Molecular Structural Biology, Max Planck Institute of Biochemistry, 82152 Martinsried, Germany. [3]Department of Biochemistry and Molecular Pharmacology, University of Massachusetts Medical School, Worcester, MA 01605, USA. [4]Cryo–Electron Microscopy, Bijvoet Center for Biomolecular Research, Utrecht University, 3584 CH Utrecht, Netherlands.
*These authors contributed equally to this work.
†Corresponding author. Email: beckmann@genzentrum.lmu.de (R.B.); pfeffer@biochem.mpg.de (S.P.); f.g.forster@uu.nl (F.F.)
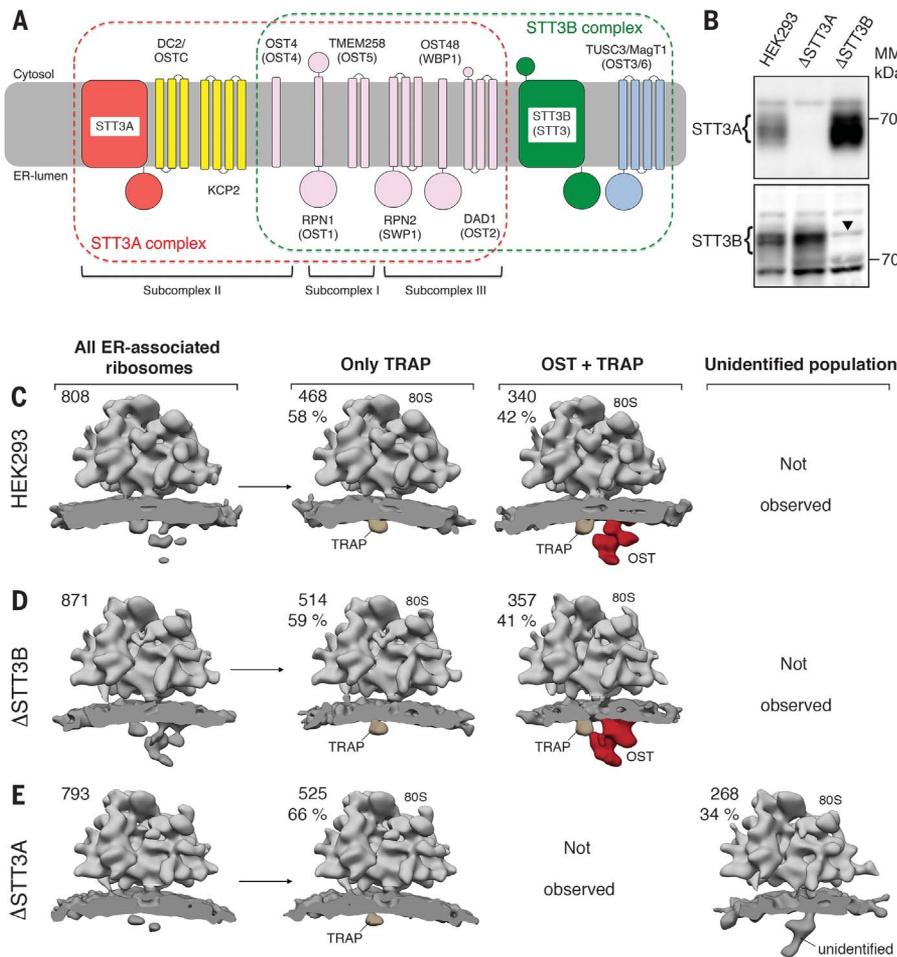
Fig. 1. RTCs harbor exclusively STT3A complexes. (**A**) Schematic representation and membrane topology of OST subunits for the STT3A (red frame) and STT3B complexes (green frame; yeast names in parentheses). Shared subunits are depicted in pink. OST subcomplexes are indicated for the STT3A complex. (**B**) Microsomes from wild-type or mutant human embryonic kidney (HEK) 293 cells were analyzed by immunoblotting using rabbit polyclonal antibodies. The arrowhead in the STT3B blot designates a nonspecific background band. MM, molecular mass. (**C** to **E**) Ribosome-bound translocon populations observed for microsomes from wild-type HEK293 (C), ΔSTT3B (D), and ΔSTT3A (E) cell lines after in silico sorting. The absolute number and percentage of subtomograms contributing to each class are given. All densities were filtered to 30-Å resolution. 80S, eukaryotic ribosome.

protein eL28 (Fig. 2, A and E). Antibodies against the cytosolic RPN1 segment inhibit protein translocation by interfering with ribosome binding to the translocon, confirming direct ribosome-RPN1 interaction (25). We further observed four extra TMs tightly associated with STT3A belonging to subcomplex II. One single TM, which we attributed to the single-spanning membrane protein OST4, was tightly intercalated between STT3A TMs 1, 3, 12, and 13 (fig. S7). The three remaining TMs located at the interface between STT3A TMs 10 to 13 and Sec61 were assigned to DC2. We built an atomic model for the three TMs of DC2 de novo based on excellent agreement between features resolved in our map and the predicted length and connectivity of DC2 TMs (Fig. 2F and fig. S3D). Recent biochemical data (10) show that

DC2 assumes a central role in recruiting OST into the translocon complex, and interactions of DC2 with both Sec61 and STT3A have been predicted. Indeed, DC2 contacted STT3A via its lumenal C terminus (to STT3A TM13) (Fig. 2F), the cytosolic TM2-TM3 loop (to STT3A TM12-TM13 loop), and TM2 (close proximity to STT3A TM9-TM10 loop, also referred to as EL5). The amphipathic DC2 N terminus projected toward Sec61 on the micelle surface (Fig. 2F), whereas the lumenal loop of DC2 interacted with the C termini of Sec61β and Sec61γ (Fig. 2F). We did not observe density for KCP2, likely because it tends to dissociate upon solubilization (10). We observed an additional weaker density for a TM segment intercalated between DC2 and Sec61 in the peptidyl-tRNA–containing map,

which was absent in the nonprogrammed map (Fig. 2, B and C, and fig. S2) and might correspond to the nascent opsin substrate or an as yet unknown translocon component.

We identified two interfaces integrating the STT3A complex into the RTC, one between the ribosome and the cytosolic RPN1 domain (Fig. 2, A and E) and one between DC2 and Sec61 (Fig. 2, B and F), both of which could explain STT3-paralog specificity. First, STT3B possesses a specific 47–amino acid soluble domain extending from STT3 TM1 into the cytosol directly beneath the cytosolic RPN1 helix bundle (Fig. 2, B and C). The STT3B-specific extension would thus be located in immediate proximity to the ribosome-OST interface, where it could interfere with ribosome binding. Second, STT3 TMs 10 to 13 and the cytosolic STT3 TM12-TM13 loop, identified as the major contact sites between DC2 and STT3A (Fig. 2, C and F), differed considerably between the STT3 paralogs (table S1 and fig. S8). This suggests that DC2 binds specifically to the STT3A paralog, which would exclude STT3B complexes from the RTC.

In our second (nonprogrammed) reconstruction (fig. S2), the general translocon architecture was very similar to the P-site tRNA–containing complex, and models for laterally closed Sec61 and OST fitted well as separate rigid bodies (Fig. 3A). Comparison with the model of the programmed RTC revealed a tilting movement between Sec61 and OST, with the cytosolic loops of Sec61 and the cytosolic RPN1 domain serving as hinge points on the ribosomal large subunit (Fig. 3B and movie S1). Furthermore, we improved image processing for an already published cryo-ET data set (18) of the native RTC with laterally opened Sec61 (fig. S9) to a resolution allowing rigid body fits of Sec61 and OST (Fig. 3A). Upon opening of the Sec61 lateral gate, the Sec61α N-terminal domain and Sec61β approached DC2. This induced a repositioning of the entire OST complex to accommodate the Sec61 conformational change (Fig. 3B and movie S1). Although the relative arrangement of DC2 and Sec61 differed substantially between the three observed conformational states, DC2 always stably interacted with Sec61. Thus, DC2 acts as a versatile module that provides robust integration of OST into the translocon complex, even under vastly differing conformational states of the translocon complex.

Our cryo-EM reconstructions define the exact position and orientation of the OST catalytic site in the context of the mammalian RTC and enable a detailed dissection of the interface between OST and the ribosome-Sec61 complex. This allowed us to interpolate the path for a nascent glycosylation substrate for cotranslational scanning on translocon-associated OST (Fig. 3C) and provided a molecular basis for STT3-paralog specificity in the RTC (Fig. 3D). The minimum distance between a TM segment at the Sec61 lateral gate and the catalytic site of STT3A was about 6.5 nm, explaining why glycosylation sites that are very close to TMs are often skipped by translocon-associated OST (26).
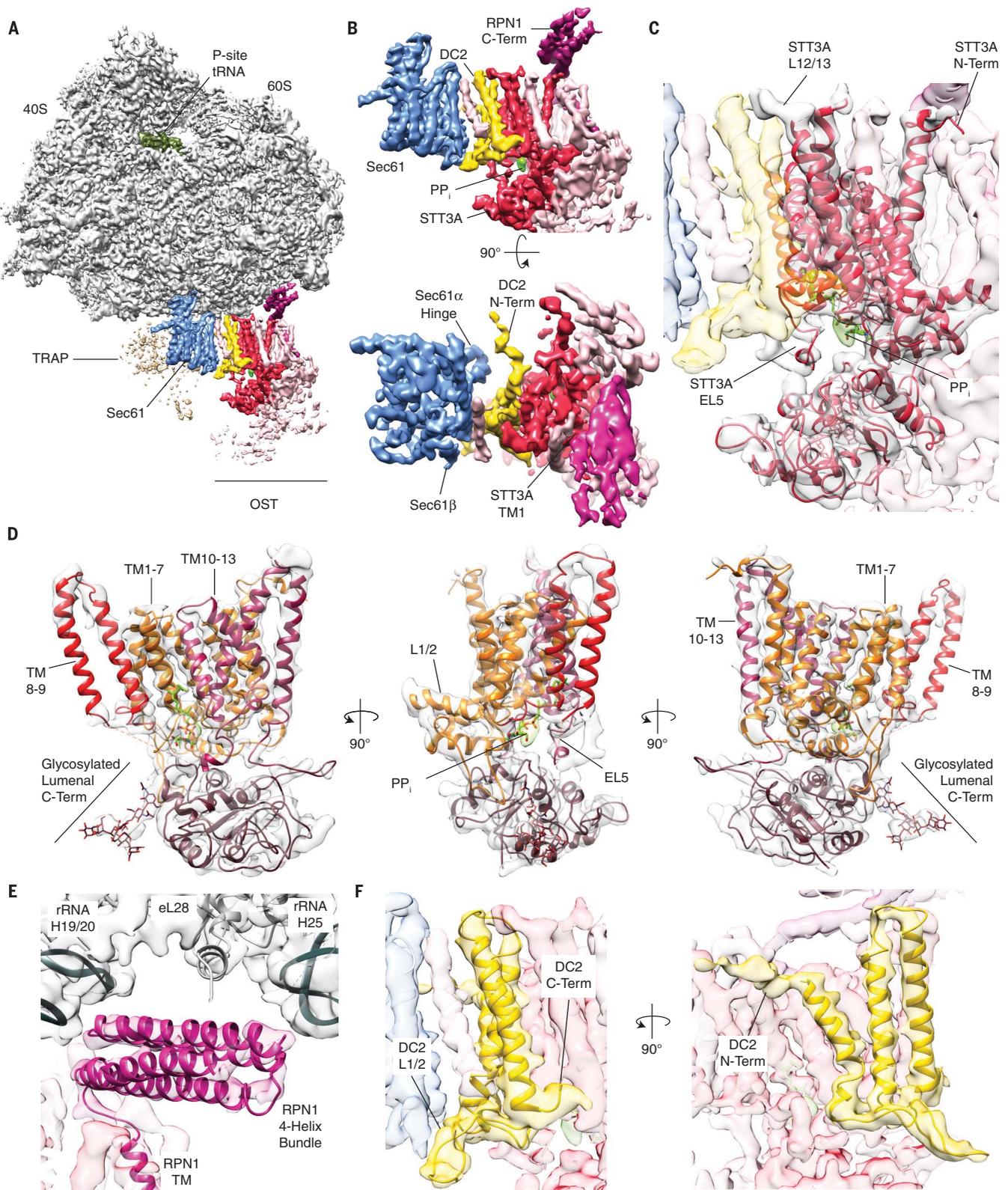
Fig. 2. Localization of STT3A, RPN1, and DC2 in ribosome-bound OST. (**A**) Cryo-EM structure of the active solubilized RTC. Ribosome and P-site tRNA are shown before focused refinement, low-pass filtered to 4 Å; the membrane region including Sec61, TRAP, and OST is shown after (fig. S2). 40*S* and 60*S* are eukaryotic ribosomal subunits. (**B**) Magnified view of the translocon region omitting TRAP, as depicted in (A) (top) or rotated by 90° (bottom). PP$_i$, inorganic pyrophosphate. (**C** and **D**) Fitted homology model for mammalian STT3A. Density for phosphate groups in the catalytic center is green. L, loop. (**E**) Magnified view of the cytosolic RPN1 four-helix bundle binding to the ribosome. (**F**) Magnified view of the Sec61-OST interface with a fitted model for the DC2 TMs.
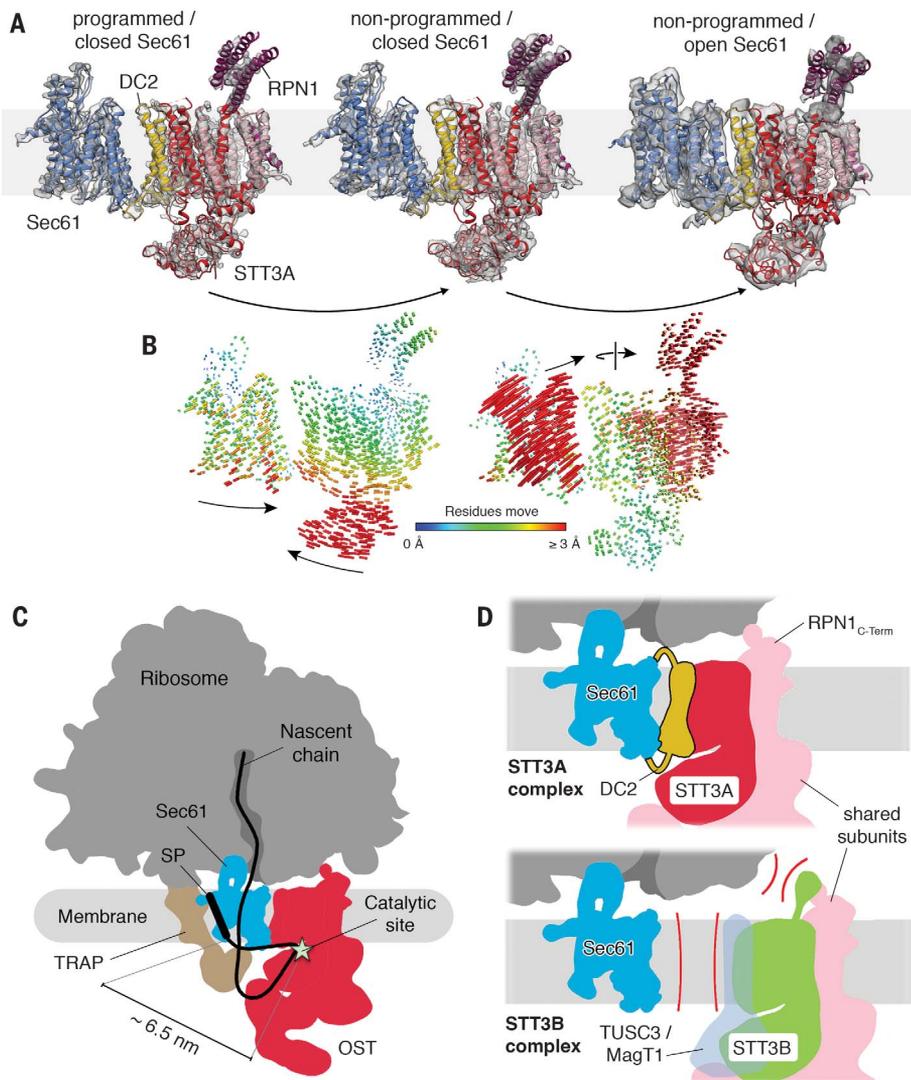
Fig. 3. Translocon dynamics and scheme for cotranslational N-glycosylation. (**A**) Models for Sec61 and OST were fitted into the RTC densities with laterally closed (left, programmed; center, nonprogrammed) and opened Sec61 (right). (**B**) Trajectories of α carbon atoms connecting the observed conformational states with color-coded length. (**C**) Schematic representation of the RTC with an interpolated example path for a nascent secretory protein. The STT3A catalytic site and a signal peptide (SP) or TM in the Sec61 lateral gate are separated by ~6.5 nm. (**D**) Molecular basis for STT3-paralog specificity in the RTC. The DC2 and RPN1 subunits tie the STT3A complex into the RTC (top). The lack of DC2 and potential interference of the STT3B-specific cytosolic domain with ribosome binding exclude STT3B complexes from the RTC (bottom).

REFERENCES AND NOTES

1. S. Pfeffer, J. Dudek, R. Zimmermann, F. Förster, *Biochim. Biophys. Acta* **1860**, 2122–2129 (2016).
2. R. M. Voorhees, R. S. Hegde, *Curr. Opin. Cell Biol.* **41**, 91–99 (2016).
3. T. A. Rapoport, L. Li, E. Park, *Annu. Rev. Cell Dev. Biol.* **33**, 369–390 (2017).
4. F. Cymer, G. von Heijne, S. H. White, *J. Mol. Biol.* **427**, 999–1022 (2015).
5. R. Beckmann *et al.*, *Science* **278**, 2123–2126 (1997).
6. E. Mohorko, R. Glockshuber, M. Aebi, *J. Inherit. Metab. Dis.* **34**, 869–878 (2011).
7. D. J. Kelleher, R. Gilmore, *Glycobiology* **16**, 47R–62R (2006).
8. M. Chavan, W. Lennarz, *Trends Biochem. Sci.* **31**, 17–20 (2006).
9. D. J. Kelleher, D. Karaoglu, E. C. Mandon, R. Gilmore, *Mol. Cell* **12**, 101–111 (2003).
10. S. Shrimal, N. A. Cherepanova, R. Gilmore, *J. Cell Biol.* **216**, 3625–3638 (2017).
11. C. Ruiz-Canada, D. J. Kelleher, R. Gilmore, *Cell* **136**, 272–283 (2009).
12. C. Lizak, S. Gerber, S. Numao, M. Aebi, K. P. Locher, *Nature* **474**, 350–355 (2011).
13. S. Matsumoto *et al.*, *Proc. Natl. Acad. Sci. U.S.A.* **110**, 17868–17873 (2013).
14. M. Napiórkowska *et al.*, *Nat. Struct. Mol. Biol.* **24**, 1100–1106 (2017).
15. R. Wild *et al.*, *Science* **359**, 545–550 (2018).
16. L. Bai, T. Wang, G. Zhao, A. Kovach, H. Li, *Nature* (2018).
17. J. Mahamid *et al.*, *Science* **351**, 969–972 (2016).
18. S. Pfeffer *et al.*, *Nat. Commun.* **6**, 8403 (2015).
19. S. Pfeffer *et al.*, *Nat. Commun.* **5**, 3072 (2014).
20. S. L. Meacock, F. J. Lecomte, S. G. Crawshaw, S. High, *Mol. Biol. Cell* **13**, 4114–4129 (2002).
21. R. M. Voorhees, I. S. Fernández, S. H. Scheres, R. S. Hegde, *Cell* **157**, 1632–1643 (2014).
22. R. M. Voorhees, R. S. Hegde, *Science* **351**, 88–91 (2016).
23. M. Gogala *et al.*, *Nature* **506**, 107–110 (2014).
24. E. Park, T. A. Rapoport, *Nature* **473**, 239–242 (2011).
25. Y. H. Yu, D. D. Sabatini, G. Kreibich, *J. Cell Biol.* **111**, 1335–1342 (1990).
26. I. M. Nilsson, G. von Heijne, *J. Biol. Chem.* **268**, 5798–5801 (1993).

Science

Structural basis for coupling protein transport and N-glycosylation at the mammalian endoplasmic reticulum

Katharina Braunger, Stefan Pfeffer, Shiteshu Shrimal, Reid Gilmore, Otto Berninghausen, Elisabet C. Mandon, Thomas Becker, Friedrich Förster and Roland Beckmann

A close-up view of oligosaccharyltransferase

Many secretory and membrane proteins are modified through the attachment of sugar chains by N-glycosylation. Such modification is required for correct protein folding, targeting, and functionality. In mammalian cells, N-glycosylation is catalyzed by the oligosaccharyltransferase (OST) complex via its STT3 subunit. OST forms a complex with the ribosome and the Sec61 protein translocation channel. Braunger *et al.* combined cryo-electron microscopy approaches to visualize mammalian ribosome-Sec61-OST complexes in order to build an initial molecular model for mammalian OST.

Science, this issue p. 215

ARTICLE TOOLS	http://science.sciencemag.org/content/360/6385/215
SUPPLEMENTARY MATERIALS	http://science.sciencemag.org/content/suppl/2018/03/07/science.aar7899.DC1
REFERENCES	This article cites 39 articles, 9 of which you can access for free http://science.sciencemag.org/content/360/6385/215#BIBL
PERMISSIONS	http://www.sciencemag.org/help/reprints-and-permissions

Use of this article is subject to the Terms of Service